

Deformation and buckling of microcapsules in a viscoelastic matrix

Amir Hossein Raffiee,¹ Sadegh Dabiri,^{1,2} and Arezoo M. Ardekani¹

¹*School of Mechanical Engineering, Purdue University, West Lafayette, Indiana 47907, USA*

²*Department of Agricultural and Biological Engineering, Purdue University, West Lafayette, Indiana 47907, USA*

(Received 10 February 2017; revised manuscript received 20 June 2017; published 6 September 2017)

In this paper, we numerically study the dynamics of (1) a Newtonian liquid-filled capsule in a viscoelastic matrix and that of (2) a viscoelastic capsule in a Newtonian matrix in a linear shear flow using a front-tracking method. The numerical results for case (1) indicate that the polymeric fluid reduces the capsule deformation and aligns the deformed capsule with the flow direction. It also narrows the range of tension experienced by the deformed capsule for case (1), while the tank-treading period significantly increases. Interestingly, the polymeric fluid has an opposite effect on the tank-treading period and the orientation angle of case (2), but its effect on the deformation is similar to case (1).

DOI: [10.1103/PhysRevE.96.032603](https://doi.org/10.1103/PhysRevE.96.032603)

I. INTRODUCTION

Extensive research on microcapsules has been documented in recent years, due to their growing applications in consumable, pharmaceutical, and medical industries. Capsules are liquid-filled droplets surrounded by an elastic membrane that are often used in targeted drug and cell delivery applications [1] and encapsulation of volatile substances in lab-on-a-chip devices [2,3]. In many of these applications, either the background fluid or encapsulated fluid are non-Newtonian due to presence of DNA, proteins, or polymers [4,5].

A large number of numerical, experimental, and theoretical studies have been conducted on the capsule behavior under various flow fields in a Newtonian fluid [6–10]. These models suggest that the motion of capsule depends on the imposed flow field, membrane stiffness, shear rate, initial shape, and viscosity ratio (the ratio of inner fluid viscosity to the outer fluid viscosity) [6,7,11]. The capsule deforms to a steady shape in a shear flow, and the membrane rotates around it, which is referred to as the tank-treading (TT) motion [12]. Theoretical analysis based on the perturbation method [13,14] predicts the deformation of initially spherical capsule in a simple shear flow of a Newtonian fluid as well as the TT motion of the membrane. The perturbation method is, however, valid only for small deformations. Therefore, numerical simulations are required to address large capsule deformations. The boundary integral, front-tracking [7,8], and immersed boundary method [9] are among the numerical techniques widely utilized for simulating the capsule dynamics in a shear flow of a Newtonian fluid. In these methods the membrane is discretized using Lagrangian grids, which enables us to accurately capture the membrane deformation and to calculate the elastic force acting on the capsule. These numerical methods have been used to investigate the role of the membrane constitutive laws, area incompressibility, and bending resistance [8,10,15]. The experimental study on synthetic capsules suspended in a confined shear flow suggests that the membrane starts thinning along the principal strain axes of the shear flow when the shear rate is sufficiently large [16]. The capsule break-up occurs in these areas [11,16]. Despite numerous studies on the deformation and TT motion of capsules in Newtonian fluids, their motion in a viscoelastic fluid is poorly studied.

In this work, we present three-dimensional numerical simulations of the dynamics of a Newtonian capsule in a

polymeric matrix following an Oldroyd-B fluid constitutive equation as well as dynamics of a polymeric capsule in a Newtonian fluid. A front-tracking method is employed to accurately capture the underlying physics of a deforming capsule in a shear flow for a wide range of capillary and Weissenberg numbers.

II. GOVERNING EQUATIONS AND NUMERICAL METHODS

A. Newtonian fluid

In this section, we first present the system of equations governing the motion of a deformable Newtonian capsule in a Newtonian fluid and the mathematical method used for capturing the interface between the elastic membrane and the surrounding fluid. We will then discuss the constitutive equation and the numerical implementation for a viscoelastic fluid. The inner and outer fluids are assumed to be incompressible. Hence, the flow field is governed by the Navier-Stokes equations:

$$\nabla \cdot \mathbf{u} = 0, \quad (1)$$

$$\frac{\partial(\rho\mathbf{u})}{\partial t} + \nabla \cdot (\rho\mathbf{u}\mathbf{u}) = -\nabla p + \nabla \cdot \boldsymbol{\tau} + \mathbf{F}, \quad (2)$$

where ρ is equal to the density of inner (outer) fluid inside (outside) the capsule, p represents the pressure, \mathbf{u} is the velocity vector, t is the time, and $\boldsymbol{\tau}$ denotes the total stress tensor. The total stress tensor for a Newtonian fluid is $\boldsymbol{\tau} = \mu\mathbf{D}$, where $\mathbf{D} = (\nabla\mathbf{u}) + (\nabla\mathbf{u})^T$ is the strain rate tensor. In this equation, $\mathbf{F}(\mathbf{x}, t) = \int_{\partial B} \mathbf{f}(\mathbf{x}_i, t)\delta(\mathbf{x} - \mathbf{x}_i)dV$ is the smoothed representation of the membrane force, which is zero everywhere except at the interface location. In this formulation, \mathbf{x} and \mathbf{x}_i denote arbitrary points on the Eulerian and Lagrangian grids, respectively, and δ and V represent the Dirac delta function and the volume. Furthermore, $\mathbf{f}(\mathbf{x}_i, t)$ is the elastic force of the membrane. The capsule membrane is modeled as an infinitely thin sheet of elastic material following a neo-Hookean constitutive equation. Therefore, the corresponding strain energy function W is expressed as

$$W = \frac{E_s}{6}(\epsilon_1^2 + \epsilon_2^2 + \epsilon_1^{-2}\epsilon_2^{-2} - 3), \quad (3)$$

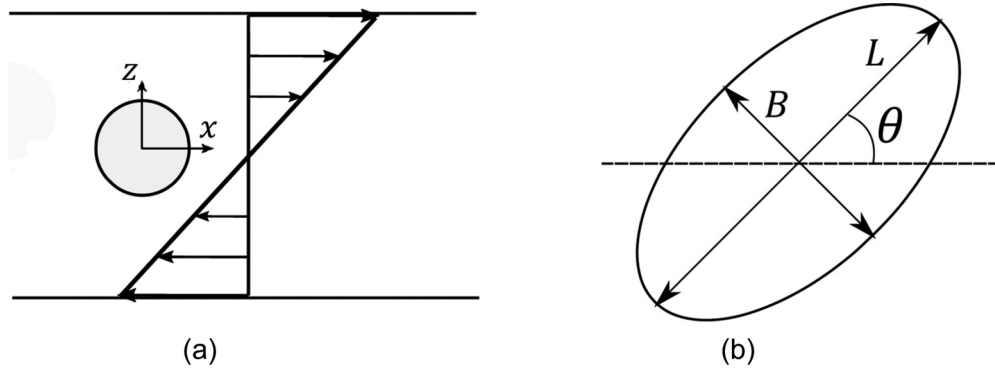


FIG. 1. Schematic of the problem and coordinate system.

where ϵ_1 and ϵ_2 are the principal strains and E_s is the two-dimensional elastic shear modulus. The elastic force on the capsule membrane is obtained using the finite element model developed by Refs. [17,18]. In this model, the membrane surface is discretized with triangular elements. The number of surface elements is large enough so that these elements remain approximately flat even after large deformations. The Lagrangian grid is deformed due to the hydrodynamic interaction with the surrounding fluid and consequently a resistive elastic force develops. The deformed and initially undeformed elements are transformed to a common two-dimensional plane to evaluate the displacement of vertices and the corresponding elastic force $[f(x_i, t)]$ exerted on the membrane using the principle of virtual work, $f = \frac{-dW}{dv}$, where v denotes the displacement of vertices between deformed and undeformed states.

In this work, a finite volume method is used to discretize the equations. The computational domain is discretized using a uniform, Cartesian, and staggered grid. The governing equations are solved in the entire domain using an explicit Euler method for time discretization, a third order Quadratic Upstream Interpolation for Convective Kinematics scheme [19] for the convective term and a central difference scheme for the diffusive term. Furthermore, the pressure-velocity coupling is conducted using a projection method [20]. A front-tracking method [21] is used to model the capsule. The Navier-Stokes equations are solved on the entire computational domain rather

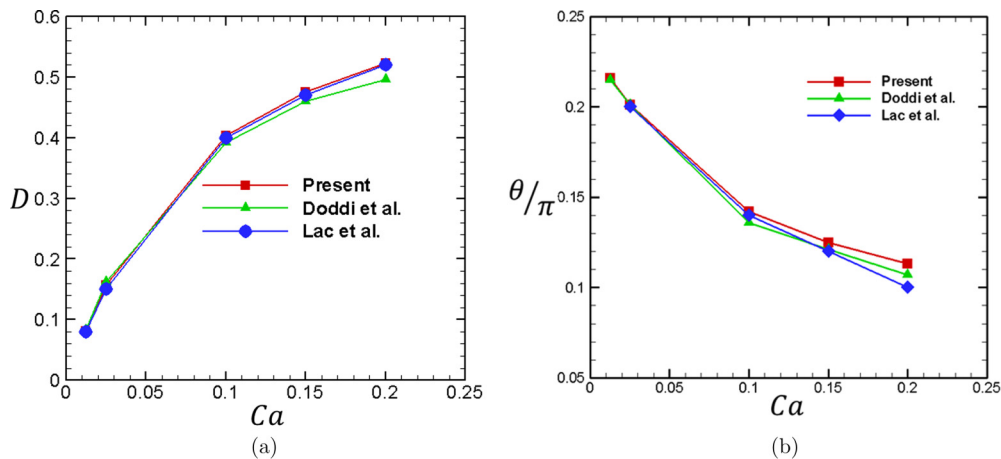
than solving them separately for each phase and matching the boundary conditions at the interface. Fluid properties (i.e., density and viscosity) are uniform in the interior and exterior fluids but sharply vary in a small region across the interface. To provide a smooth representation of material properties, we solve Poisson's equation for an indicator function, which is used to evaluate fluid properties everywhere in the computational domain. The elastic force is evaluated on the Lagrangian marker points on the interface and are added as a singular body force in the momentum equation to account for the presence of membrane. The velocity field on Lagrangian points are calculated as

$$u(x_i) = \int u(x)\delta(x - x_i) dV. \quad (4)$$

This method requires an interpolation for treating the singular body force in Eq. (2) and tracking the membrane temporal evolution. Therefore, a smoothed representation of the delta function is employed to distribute the desired variables with sharp variation across the interface over few grid points surrounding the interface:

$$\delta(x) = D(x)D(y)D(z), \quad (5)$$

$$D(x) = \frac{1}{4\Delta} \left\{ 1 + \cos \left[\frac{\pi}{2\Delta}(x) \right] \right\}, \quad |x| \leq 2\Delta, \quad (6)$$


 FIG. 2. A comparison of the (a) capsule deformation parameter and (b) orientation angle with the results of Doddi *et al.* [24] and Lac *et al.* [23].

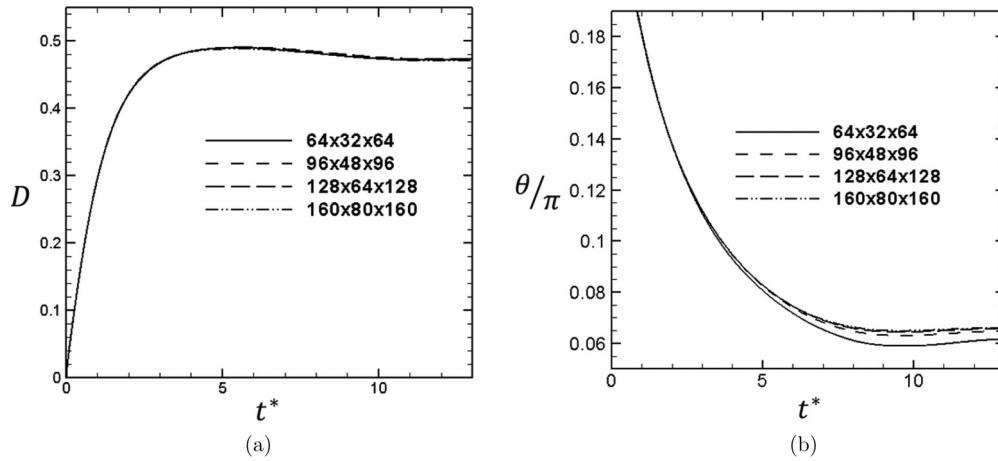


FIG. 3. Temporal evolution of the (a) capsule deformation and (b) transient orientation angle at $Ca = 0.2$ and $Wi = 2$.

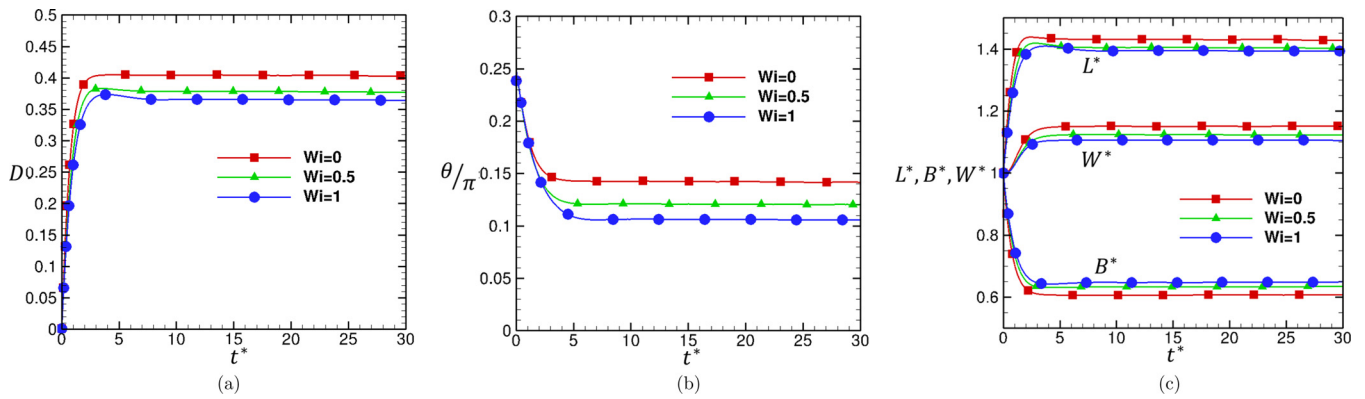


FIG. 4. Temporal evolution of the (a) capsule deformation, (b) orientation angle, and (c) length of main axes at $Ca = 0.1$.

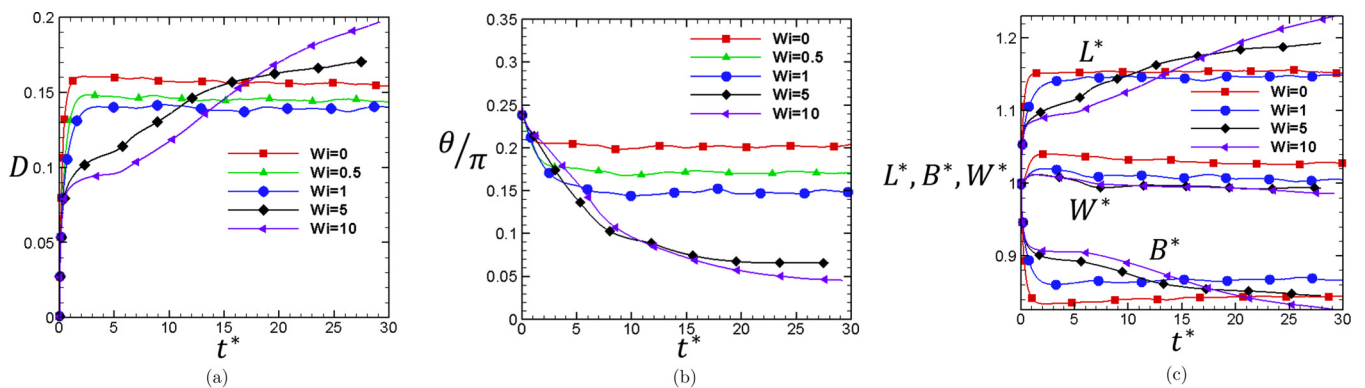


FIG. 5. The temporal evolution of the (a) capsule deformation, (b) orientation angle, and (c) axes length for $Ca = 0.025$.

where Δ is the grid size. In summary, a single set of equations is solved in the entire computational domain, taking into account the presence of the membrane and changes in the fluid properties across the interface.

B. Non-Newtonian fluid

The Oldroyd-B constitutive equation is used to describe the polymeric stress in the inner and outer fluid. The total stress tensor $\boldsymbol{\tau}$ is decomposed into solvent $\boldsymbol{\tau}_s$ and viscoelastic $\boldsymbol{\tau}_p$ stress tensors as follows:

$$\boldsymbol{\tau} = \boldsymbol{\tau}_p + \boldsymbol{\tau}_s, \quad (7)$$

where

$$\boldsymbol{\tau}_s = \mu_s \mathbf{D}, \quad (8)$$

$$\lambda \overset{\nabla}{\boldsymbol{\tau}}_p + \boldsymbol{\tau}_p = \mu_p \mathbf{D}. \quad (9)$$

In this formulation, μ_s and μ_p are the solvent and polymer viscosity, respectively. The polymer relaxation time, represented by λ , is zero when the fluid is Newtonian and has a nonzero value when the fluid is viscoelastic. $\overset{\nabla}{\boldsymbol{\tau}}_p$ denotes the upper convected time derivative defined as

$$\overset{\nabla}{\boldsymbol{\tau}}_p = \frac{\partial \boldsymbol{\tau}_p}{\partial t} + \mathbf{u} \cdot \nabla \boldsymbol{\tau}_p - \nabla \mathbf{u} \boldsymbol{\tau}_p - \boldsymbol{\tau}_p \nabla \mathbf{u}^T. \quad (10)$$

We follow the implementation of Aggarwal *et al.* [22] for the polymeric stress to implement a single constitutive equation in the entire computation domain:

$$\lambda \frac{\partial \boldsymbol{\tau}_p}{\partial t} + \boldsymbol{\tau}_p = K(t), \quad (11)$$

where

$$K(t) = \mu_p \mathbf{D} - \lambda (\mathbf{u} \cdot \nabla \boldsymbol{\tau}_p - \nabla \mathbf{u} \boldsymbol{\tau}_p - \boldsymbol{\tau}_p \nabla \mathbf{u}^T). \quad (12)$$

This equation is discretized using an explicit Euler scheme for time:

$$\begin{aligned} \boldsymbol{\tau}_p(t + \Delta t) &= \boldsymbol{\tau}_p(t) \exp\left(-\frac{\Delta t}{\lambda}\right) + K(t + \Delta t) - K(t) \\ &\times \exp\left(-\frac{\Delta t}{\lambda}\right) - \exp\left(-\frac{(t + \Delta t)}{\lambda}\right) \\ &\times \int_t^{t+\Delta t} \exp\left(\frac{t}{\lambda}\right) \frac{\partial K}{\partial t} dt. \end{aligned} \quad (13)$$

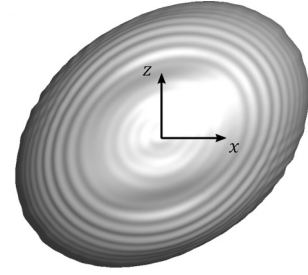
We can neglect the integral in Eq. (13) assuming $\frac{\partial K}{\partial t} = 0$. In this case, the polymeric stress tensor can be written as

$$\boldsymbol{\tau}_p^{n+1} = \boldsymbol{\tau}_p^n \exp\left(-\frac{\Delta t}{\lambda}\right) + K^n \left[1 - \exp\left(-\frac{\Delta t}{\lambda}\right)\right] \quad (14)$$

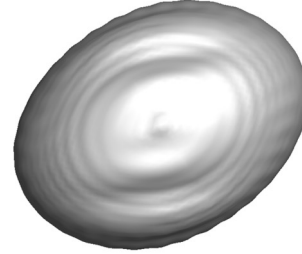
where n is the time step index.

III. PROBLEM SETUP

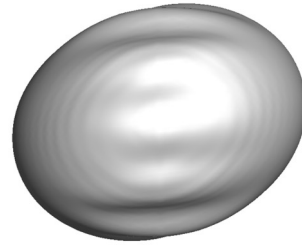
In this study, we simulate the deformation of an initially spherical, unstressed capsule, which is introduced to the flow at time $t = 0$. The capsule is deformed under a linear shear flow bounded by two infinitely long flat plates as shown in Fig. 1. Accordingly, the undisturbed velocity field in the absence of



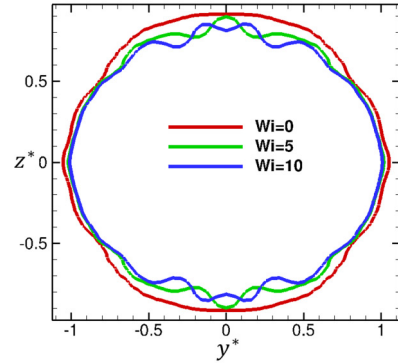
(a)



(b)



(c)



(d)

FIG. 6. Deformation of the capsule membrane at $Ca = 0.025$ and (a) $Wi = 0$, (b) $Wi = 5$, (c) $Wi = 10$, and (d) cross section of the capsule membrane for different Weissenberg numbers at $x^* = 0$.

the capsule is described as

$$U = \dot{\gamma} \left(z - \frac{H}{2}\right), \quad V = W = 0, \quad (15)$$

where U, V , and W denote the velocity of the fluid in the streamwise direction (x), wall normal direction (z), and vorticity direction (y), respectively. In this formulation, $\dot{\gamma}$ and H represent the imposed shear rate and the distance between the parallel walls. The computational domain is a

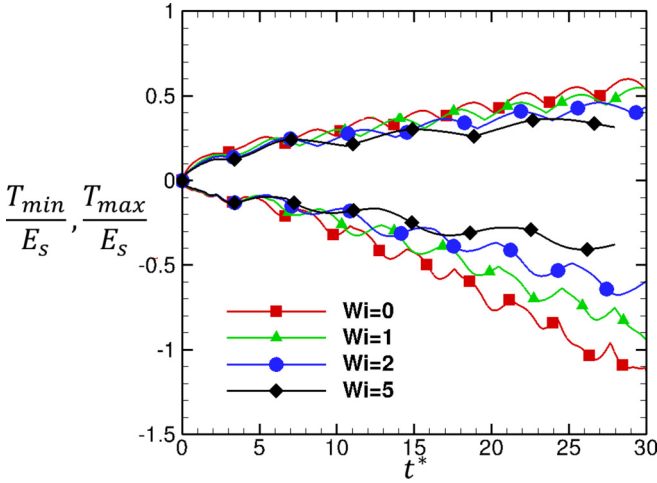


FIG. 7. The temporal evolution of maximum and minimum principal tensions at $Ca = 0.025$.

rectangular box with the size of $10R \times 5R \times 10R$ (R is the initial capsule radius) in the streamwise, wall normal, and vorticity directions, respectively. The computational domain is discretized using a uniformly distributed $128 \times 64 \times 128$ Eulerian grid points. The capsule membrane is also discretized with 8120 triangular elements. A periodic boundary condition is imposed in x and y directions, and a no-slip boundary condition is considered on the upper and lower walls. The interior fluid of the capsule is incompressible and Newtonian, while the exterior fluid is viscoelastic, following an Oldroyd-B constitutive equation. The characteristic length and time scales are R and $\dot{\gamma}^{-1}$, respectively, leading to the following dimensionless parameters: (1) Reynolds number $Re = \frac{\rho \dot{\gamma} R^2}{\mu}$, which represents the ratio of the inertial force to the viscous force, (2) capillary number $Ca = \frac{\mu \dot{\gamma} R}{E_s}$, denoting the ratio of the viscous force to the elastic force on the capsule membrane, (3) Weissenberg number $Wi = \lambda \dot{\gamma}$, and (4) $\beta = \frac{\mu_p}{\mu}$, indicating the ratio of the polymer viscosity to the total viscosity. The total viscosity is defined as the sum of polymer viscosity and solvent viscosity of the fluid ($\mu = \mu_p + \mu_s$). The interior and exterior fluids are assumed to have the same density and total viscosity. The values of β and Re are set to $\beta = 0.5$ and $Re = 0.1$, unless otherwise stated. Superscript $*$ is used to identify dimensionless time and length.

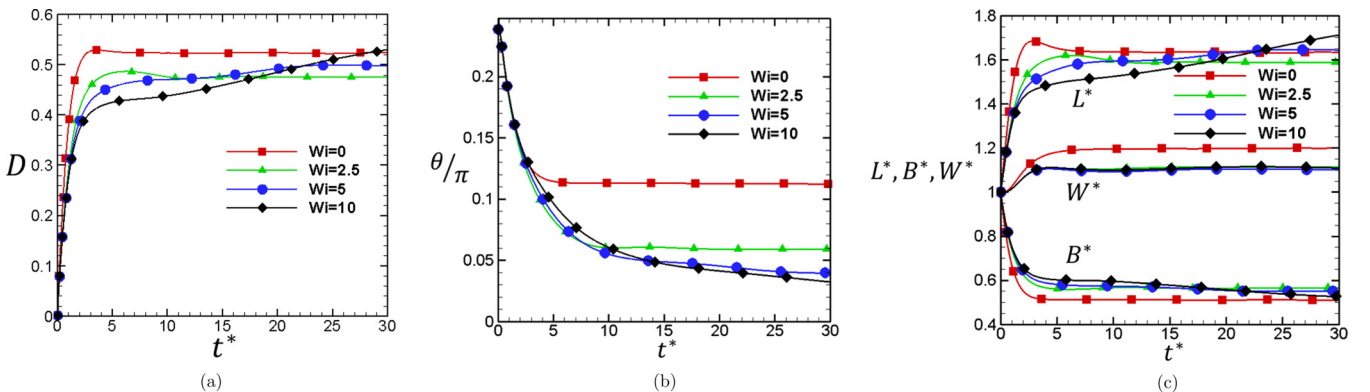


FIG. 8. The temporal evolution of the (a) capsule deformation, (b) orientation angle, and (c) axes length for $Ca = 0.2$.

IV. NUMERICAL VERIFICATION

In this section, we compare our numerical results against previously published numerical results of Refs. [23,24], where front-tracking and boundary element methods were used, respectively. For this purpose, we simulate the deformation of a neo-Hookean membrane in a linear shear flow, where the interior and exterior fluids are Newtonian. In order to conduct a quantitative comparison, the Taylor deformation parameter $D = (L - B)/(L + B)$ and orientation angle θ are evaluated, where L and B are the major and minor axes of the deformed capsule in the shear plane, respectively, and θ represents the angle between the major axis of ellipsoid and the x axis. Figure 2 shows steady-state values of deformation parameter D and orientation angle θ for various Ca . The results agree well with the published results in the literature.

The numerical convergence of the solution is investigated by increasing the grid resolution from $64 \times 32 \times 64$ to $160 \times 80 \times 160$. The temporal evolution of the deformation parameter and orientation angle for $Ca = 0.2$ and $Wi = 2$ are shown in Fig. 3. This figure shows that the capsule deformation does not depend on the grid resolutions used here, while the orientation angle converges by increasing the grid resolution. Henceforth, we choose $128 \times 64 \times 128$ grid points.

V. TRANSIENT DYNAMICS OF A VISCOELASTIC CAPSULE IN A NEWTONIAN FLUID

When the capsule is released at the center of a linear shear flow, the membrane deforms and elongates due to the hydrodynamic interaction with the surrounding fluid. The deformation grows until it reaches a steady state, when no further change is observed in the final deformed shape and inclination angle. The Lagrangian nodes on the capsule continuously rotate on the deformed capsule which is called TT mode. The temporal evolution of three main axes of the deformed membrane ($L^* = \frac{L}{R}$, $B^* = \frac{B}{R}$ and $W^* = \frac{W}{R}$) are plotted in Fig. 4(c) for $Ca = 0.1$ and various values of Wi . In this plot, L^* is the dimensionless semimajor axis and B^* is the dimensionless semiminor axis in the shear plane, and W^* denotes the dimensionless semiaxis of the capsule in the vorticity direction. The capsule elongates in two directions and compresses in the wall normal direction for both Newtonian and viscoelastic fluids. It should be noted that increase in Wi hinders stretching of L^* and W^* as well as the compression

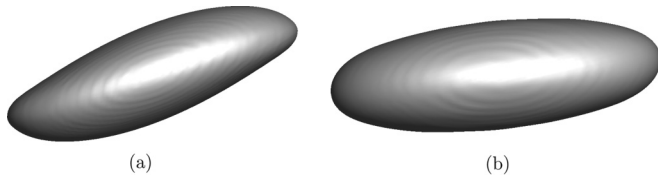


FIG. 9. Deformed capsule at $Ca = 0.2$ and (a) $Wi = 0$ and (b) $Wi = 5$.

of B^* . This means that the surrounding viscoelastic fluid reduces the capsule deformation and orientation angle due to large polymeric stresses developed in the outer fluid [Figs. 4(a)–4(b)]. As illustrated in Fig. 4(a), an overshoot is observed in the deformation of the membrane when the outer fluid is viscoelastic at $Wi = 0.5$ and 1. This phenomenon is attributed to the relaxation time of the outer viscoelastic fluid leading to a delay in the development of the polymeric stress. Consequently, the membrane deformation is larger than its steady values. Additionally, as the Weissenburg number increases, the orientation angle of the capsule in a shear flow decreases, and it reaches the equilibrium state at a longer time.

A. Capsule deformation in a low capillary number regime

In this section, we investigate the dynamics of a sheared capsule in a low capillary number regime. The temporal evolution of the capsule deformation parameter for different Weissenburg numbers at $Ca = 0.025$ is shown in Fig. 5(a). The deformation increases and reaches an equilibrium value, following by small-amplitude oscillations. These oscillations are caused by the formation of folds on the membrane surface, which is discussed later in this section. The membrane deformation in this low capillary number regime decreases with Weissenburg number similar to the observation in the previous section. However, the fluid elasticity does not have the same effect for the entire range of Wi considered here. The reduction in the steady deformation is observed for $Wi \in [0, 2]$. On the other hand, the capsule deformation monotonically increases with time for larger Wi numbers (e.g., $Wi = 5$). This behavior was also observed for droplets suspended in a shear flow. The reason for this unexpected behavior can be attributed to the memory and nonlinearity of the Oldroyd-B fluid [22] as

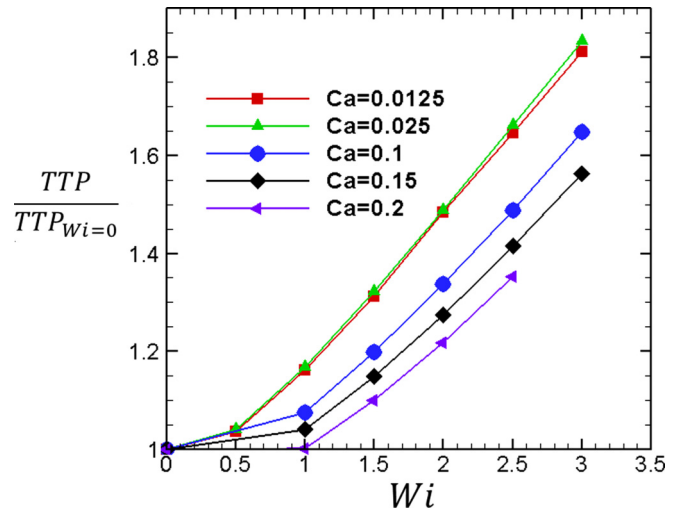


FIG. 11. The normalized value of the tank treading period versus Wi .

a similar trend exists for the variation of the drag coefficient of a cylinder with increasing Wi [25]. In order to explore the deformation of capsule in more detail, the transient lengths of major and minor axes are plotted in Fig. 5(c). The elongation of L^* and compression of B^* decreases for cases with steady-state deformations. However, at $Wi = 5$, L^* and B^* monotonically increase with time, while the vorticity-directed axis (W^*) has an infinitesimal change in this case. Increase in the fluid elasticity causes the capsule to get more aligned with the flow direction. The orientation angle monotonically decreases with the Weissenburg number for the entire range of Wi investigated in this work. This is in contrast to the elasticity effects on the deformation where it decreases for low Weissenburg numbers, but is unstable for Wi above a certain threshold. The folds on the capsule surface are illustrated in Fig. 6 for various Wi .

One of the important parameters in cell biology is the maximum tension experienced by the cell membrane. If maximum tension exceeds a threshold, the cell membrane bursts and releases its contents, which has harmful effects on the function of biological systems. The effects of principal tension

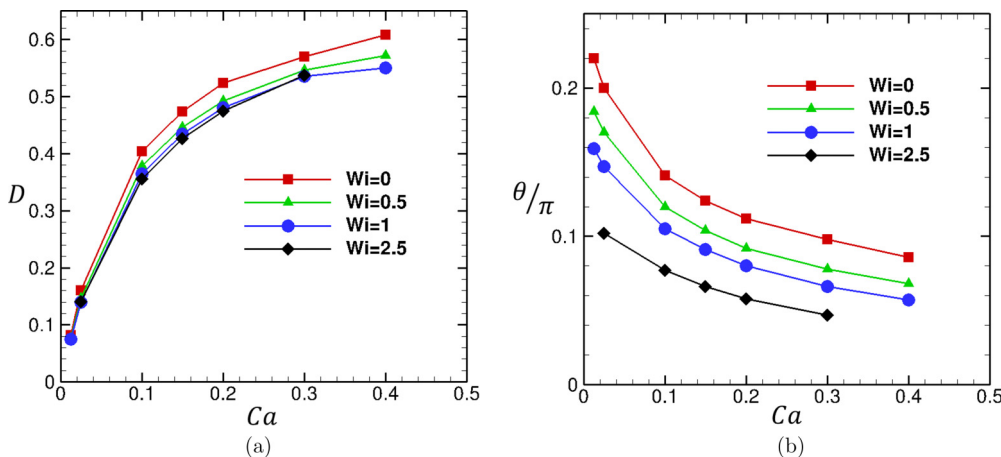


FIG. 10. (a) The capsule deformation and (b) inclination angle versus capillary number.

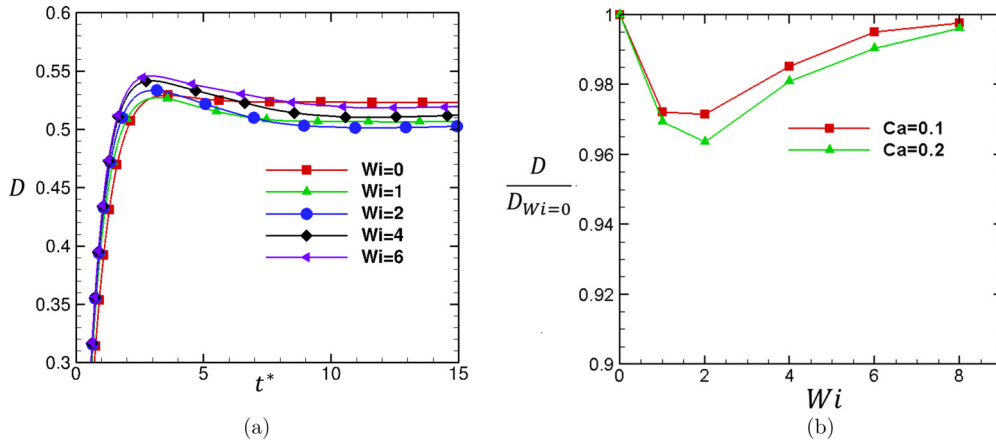


FIG. 12. Temporal evolution of (a) deformation for $Ca = 0.2$ and (b) normalized deformation as a function of Wi .

on mechanotransduction of biological cells have become the subject of recent studies [26]. Therefore, it is important to study the evolution of maximum and minimum tension on the membrane. To do so, the principal elastic tensions are computed on each triangular element on the membrane, which is used to evaluate the range of experienced tension at each time step. According to Li *et al.* [7] the principal tension on each element, represented by T_1 and T_2 , are explicitly written as

$$T_1 = \frac{1}{\epsilon_2} \frac{dW}{d\epsilon_1} = \frac{E_s}{3\epsilon_1\epsilon_2} (\epsilon_1^2 - \epsilon_1^{-2}\epsilon_2^{-2}), \quad (16)$$

$$T_2 = \frac{1}{\epsilon_1} \frac{dW}{d\epsilon_2} = \frac{E_s}{3\epsilon_1\epsilon_2} (\epsilon_2^2 - \epsilon_1^{-2}\epsilon_2^{-2}). \quad (17)$$

By finding the values of T_1 and T_2 on each element the maximum and minimum principal tension on the membrane can be computed. The temporal evolution of maximum and minimum tensions for different Wi at $Ca = 0.025$ is illustrated in Fig. 7. The increase in Wi decreases the maximum and increases the minimum tensions, indicating that the range of tension experienced by the capsule decreases with Wi .

B. Capsule deformation in a moderate capillary number regime

The deformation of a capsule is plotted in Fig. 8(a) for $Ca = 0.2$ and various Wi . Numerical simulations predict that the steady-state deformation decreases with increasing Wi number. This behavior changes for larger Wi number such that the deformation starts increasing with increasing fluid elasticity. The reason for this complex phenomenon is the nonlinearity of the fluid as discussed in the previous section. The temporal evolution of orientation angle, plotted in Fig. 8(b), shows the effect of fluid elasticity on the membrane inclination angle. The deformed shape of the capsule in Newtonian and viscoelastic surrounding fluids is represented in Fig. 9. The resulting membrane develops high-curvature tips due to the large viscous stretching exerted by the flow field on the membrane in a Newtonian fluid, while these tips are less sharp as Wi increases. This phenomenon is more prominent for larger Wi . The effect of fluid elasticity on the deformation and orientation angle are shown in Fig. 10. The deformation increases with Ca as expected, and fluid elasticity reduces the capsule deformation particularly for large Wi . The effect of the fluid elasticity on the deformation is negligible at small Ca , but it has a significant effect on the orientation angle. The capsule aligns more with the flow direction as fluid elasticity increases. In order to study TT behavior of a deformed capsule the

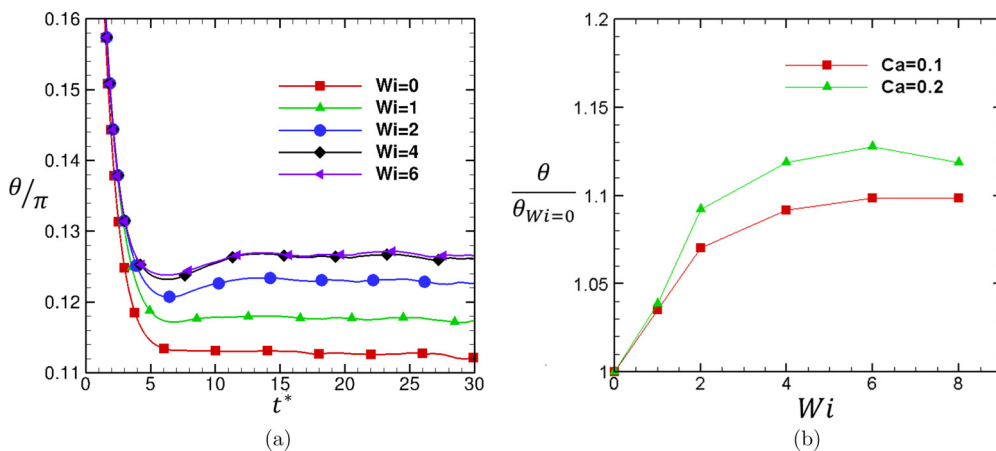


FIG. 13. Temporal evolution of (a) orientation angle for $Ca = 0.2$ and (b) normalized orientation angle as a function of Wi .

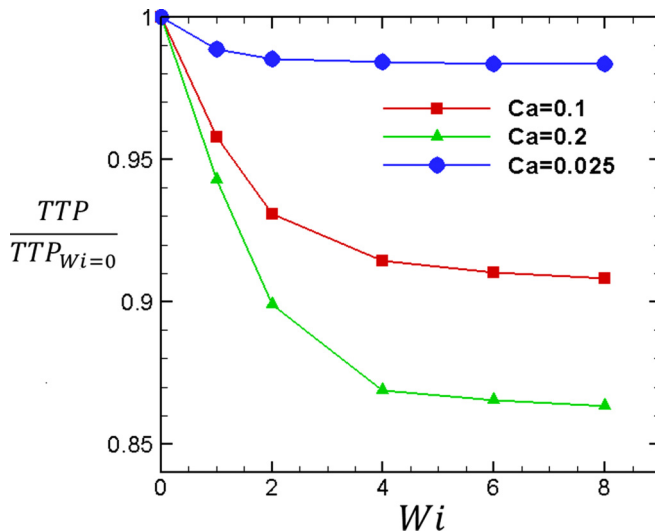


FIG. 14. The normalized value of TTP versus Wi .

tank-treading period (TTP) is defined as the time required by the material points on the membrane to complete a circulation. Therefore, we choose an arbitrary material point located on the shear plane and track its position and angle with the x direction to quantify the time period. Figure 11 shows the effect of Wi on the TTP compared to the one in a Newtonian fluid. This ratio is always larger than unity, which implies that the fluid elasticity of the outer fluid slows down the rotational velocity of the deformed membrane leading to a larger TTP. As we know, the TTP in a Newtonian fluid is prolonged at higher Ca because the membrane is highly deformed and the material points circulate a larger distance to complete an orbit. According to Fig. 11, the relative change in TTP caused by fluid elasticity reduces as Ca increases.

VI. VISCOELASTIC CAPSULE IN A NEWTONIAN MATRIX

In this section, we investigate the dynamics of a viscoelastic liquid-filled capsule suspended in a Newtonian fluid. The effect of inner polymeric fluid on the deformation is shown in Fig. 12 for a range of Wi . The steady value of deformation decreases for $Wi \in [0, 2]$ and increases for any value outside of this range [Figs. 12(a) and 12(b)]. Furthermore, the overshoot observed in the deformation parameter can be attributed to the polymer relaxation time as explained in the previous section. The effect of the inner viscoelastic fluid is of the order of 3%–4% on the deformation parameter, which proves negligible effects of fluid elasticity compared to the case where the outer fluid is

viscoelastic [Fig. 12(b)]. The viscoelastic fluid is bounded in a finite volume of capsule and cannot have a significant effect on the deformation parameter as that of the previous cases. On the other hand, the fluid elasticity has a more appreciable effect on the angle as shown in Fig. 13. Contrary to the deformation, polymer increases the orientation angle for $Wi \leq 6$ for $Ca = 0.2$ [Figs. 13(a) and 13(b)]. The effect of fluid elasticity on the orientation angle of the deforming capsule is enhanced for larger Ca [Fig. 13(b)]. The TTP of the viscoelastic capsule is shown in Fig. 14. Interestingly, this parameter decreases in the presence of inner fluid elasticity, which indicates faster rotational velocity of the capsule membrane. This behavior is opposite to the effect of fluid elasticity on the TTP when the outer fluid is viscoelastic. As the Ca increases, the TTP decreases more significantly compared to that of a Newtonian fluid.

VII. CONCLUSION

We have simulated a Newtonian capsule in a viscoelastic matrix as well as a viscoelastic capsule in a Newtonian matrix to investigate the role of fluid elasticity on the dynamics of a deformed capsule suspended in a shear flow. The deformation of the sheared capsule is such that the major axis in the shear plane and the axis in the vorticity direction are elongated, while the minor axis in the shear plane is compressed. The numerical results show that the outer fluid elasticity reduces the capsule deformation and orientation angle of the capsule with the streamwise direction. The capsule has a steady-state deformation for low Weissenberg numbers, and when Wi exceeds a threshold, the capsule deformation increases with time. Furthermore, the deformation curves display small-amplitude oscillations in the low capillary regime, which is due to the folds developed on the capsule membrane. Other important parameters investigated in this work are the maximum and the minimum tensions experienced by the capsule. According to the results, the range of the tension generated on the membrane decreases with Wi . The TTP calculated for the deforming capsule increases with Wi . This means that the fluid elasticity slows the rotational velocity of the membrane, and this effect is more prominent for smaller Ca . The numerical results for a viscoelastic liquid-filled capsule in a Newtonian matrix also indicate the decrease in the deformation with Wi , but interestingly the TTP and orientation angle increase, which is opposite to the capsule dynamics observed in a viscoelastic matrix.

ACKNOWLEDGMENT

This research was partially supported by a grant from National Science Foundation CBET-445955-CAREER.

-
- [1] T. Chang, W. Kühtreiber, R. P. Lanza, and W. L. Chick, *Cell Encapsulation Technology and Therapeutics* (Springer Science & Business Media, New York, 2013).
- [2] J. P. Beech, S. H. Holm, K. Adolfsson, and J. O. Tegenfeldt, *Lab Chip* **12**, 1048 (2012).
- [3] H. Bow, I. V. Pivkin, M. Diez-Silva, S. J. Goldfless, M. Dao, J. C. Niles, S. Suresh, and J. Han, *Lab Chip* **11**, 1065 (2011).
- [4] M. V. Kameneva, Z. J. Wu, A. Uraysh, B. Repko, K. N. Litwak, T. R. Billiar, M. P. Fink, R. L. Simmons, B. P. Griffith, and H. S. Borovetz, *Biorheology* **41**, 53 (2004).
- [5] H. L. Greene, R. F. Mostardi, and R. F. Nokes, *Polym. Eng. Sci.* **20**, 499 (1980).
- [6] D. Barthes-Biesel, A. Diaz, and E. Dhenin, *J. Fluid Mech.* **460**, 211 (2002).

- [7] X. Li and K. Sarkar, *J. Comput. Phys.* **227**, 4998 (2008).
- [8] S. Ramanujan and C. Pozrikidis, *J. Fluid Mech.* **361**, 117 (1998).
- [9] C. D. Eggleton and A. S. Popel, *Phys. Fluids* **10**, 1834 (1998).
- [10] M. Kraus, W. Wintz, U. Seifert, and R. Lipowsky, *Phys. Rev. Lett.* **77**, 3685 (1996).
- [11] D. Barthes-Biesel, *Physica A* **172**, 103 (1991).
- [12] H. Schmid-Schönbein and R. Wells, *Science* **165**, 288 (1969).
- [13] D. Barthes-Biesel and J. Rallison, *J. Fluid Mech.* **113**, 251 (1981).
- [14] D. Barthes-Biesel, *J. Fluid Mech.* **100**, 831 (1980).
- [15] X. Li, D. Barthes-Biesel, and A. Helmy, *J. Fluid Mech.* **187**, 179 (1988).
- [16] K. Chang and W. Olbricht, *J. Fluid Mech.* **250**, 609 (1993).
- [17] J. Charrier, S. Shrivastava, and R. Wu, *J. Strain Anal. Eng. Des.* **24**, 55 (1989).
- [18] S. Shrivastava and J. Tang, *J. Strain Anal. Eng. Des.* **28**, 31 (1993).
- [19] B. P. Leonard, *Comput. Methods Appl. Mech. Eng.* **19**, 59 (1979).
- [20] A. J. Chorin, *Math. Comput.* **22**, 745 (1968).
- [21] S. O. Unverdi and G. Tryggvason, *J. Comput. Phys.* **100**, 25 (1992).
- [22] N. Aggarwal and K. Sarkar, *J. Fluid Mech.* **584**, 1 (2007).
- [23] E. Lac, D. Barthes-Biesel, N. Pelekasis, and J. Tsamopoulos, *J. Fluid Mech.* **516**, 303 (2004).
- [24] S. K. Doddi and P. Bagchi, *Int. J. Multiphase Flow* **34**, 966 (2008).
- [25] S. B. Pillapakkam and P. Singh, *J. Comput. Phys.* **174**, 552 (2001).
- [26] K. Yoshimura, J. Usukura, and M. Sokabe, *Proc. Natl. Acad. Sci. USA* **105**, 4033 (2008).